# Supplementary Information for

# Non-monotonic Changes in Asian Water Towers' streamflow at increasing Warming Levels

Content of the SI:

## Supplementary Methods

### Calculation of potential evapotranspiration (PET) based on the CMIP6 model output

We adopt the method developed by Van Pelt et al. (2009)[1] to calculate PET based on daily temperature as follows:

$$PET=[1+\alpha_0(T-\bar{T}_0)]\cdot\overline{PET}_0 \quad (1)$$

where $\bar{T}_0$ and $\overline{PET}_0$ are the daily mean temperature (in °C) and potential evapotranspiration (in mm day$^{-1}$) for the calendar month during the period 1961-2001 (provided by the WFD), respectively; $T$ is the daily temperature from the CMIP6 model output (in °C); $\alpha_0$ is determined for each calendar month by regressing the WFD-based PET to daily temperature over each grid.

### Model physics of the modified THREW

A modified version of the Tsinghua Representative Elementary Watershed (THREW) is adopted in this study. The modified THREW that couples the modules of snowpack and glacier evolution is adopted in this study. The snow water equivalent (SWE) and snow cover area (SCA) is updated based on the following equations (also see ref 2, 3, 4)

$$M_s=\begin{cases} DDF_s\cdot(T-T_{s0}) & \text{for } T>T_{s0} \\ 0 & \text{for } T\le T_{s0} \end{cases} \quad (2)$$

$$P_s=\begin{cases} 0 & for\ T>T_s \\ P & for\ T\le T_s \end{cases} \quad (3)$$

$$\frac{dSWE}{dt}=P_s-M_s \quad (4)$$

$$SCA=A\left(\frac{SWE}{WMAX}\right)^{LL} \quad (5)$$

where $M_s$ is the snowmelt amount from the snowpack (in mm); $T$ is air temperature (in °C); $T_{s0}$ refers to the temperature threshold above which snow starts to melt (in °C); $DDF_s$ is the degree-day factor for snow, representing the snow melt rate (in mm °C$^{-1}$ day$^{-1}$); $P_s$ is the amount of snow (in mm), and is determined

by a temperature threshold $T_s$ (in °C); $A$, $WMAX$ (in mm) and $LL$ are parameters used in the snow cover depletion curve to calculate $SCA$ (in km$^2$) according to $SWE$ (in mm).

To simulate the evolution of glaciers, an algorithm proposed by Luo et al. (2013)[5] is adopted to measure the changes of glacier mass. The simulated glacier mass balance components include mass accumulation, melting of ice and snow, and refreezing of these melt water. The ice and snow melt is simulated using the degree-day factor approach introduced by Hock et al. (2005)[6]. Based on the entire glacier mass balance, the glacier volume is calculated. The glacier area is updated using the glacier volume-area scaling relation introduced by Chen and Ohmura (1990)[7] (Equation 12).

The initial glacier extent within China is determined based on the First Chinese Glacier Inventory (CGI-1)[8]. For the regions outside China, we derive the initial glacier extent based on the Randolph Glacier Inventory Version 6.0 (RGI6.0)[9] and the estimated annual glacier changes rate (0.04-1.57%/yr) (see ref [10, 11, 12] for details). The Second Chinese Glacier Inventory (SCGI) and RGI6.0 are used to validate the capability of the THREW model in capturing the dynamical changes of the glacier extent. The initial glacier thickness is computed based on an area-volume scaling relationship, and is constrained based on Millan et al. (2022)[13].

In this study, each Representative Elementary Watershed (REW) is divided into different elevation bands with an equal interval of 200 meters. This is used to consider the spatial heterogeneity in meteorological forcing. The glacier regions within an elevation band are regarded as a glacier unit (GREW). For each GREW, the glacier change is simulated using the glacier module similar to the one that is successfully incorporated into the SWAT model by Luo et al. (2013)[5]. The equations are as follows.

$$P_{sg}=\begin{cases}0 & for\ T>T_{sg}\\ P & for\ T\le T_{sg}\end{cases} \tag{6}$$

$$M_{sg}=\begin{cases}DDF_s\cdot(T-T_{s0}) & \text{for } T>T_{s0}\\ 0 & \text{for } T\le T_{s0}\end{cases} \tag{7}$$

$$Eng=\beta\cdot Ws \tag{8}$$

$$\frac{dWs}{dt} = P_{sg} - M_{sg} - E_{ng} \quad (9)$$

$$M_g = \begin{cases} 0 & \text{for } Ws>0 \\ DDF_g \cdot (T - T_{g0}) & \text{for } Ws=0,\ T>T_{g0} \\ 0 & \text{for } Ws=0,\ T \leqslant T_{g0} \end{cases} \quad (10)$$

$$\frac{dH_g}{dt} = P_{sg} - M_{sg} - M_g \quad (11)$$

$$A_g = \left(\frac{V_g}{m_g}\right)^{\frac{1}{n_g}} = \left(\frac{H_g \cdot 10^{-3} A_{g0}}{m_g}\right)^{\frac{1}{n_g}} \quad (12)$$

where Equations (6) and (7) simulate the processes of snowfall and snowmelt for the glacier areas, similar to Equations (2) and (3). $Eng$ is the amount of snow transferring to ice (in mm), which is assumed as a ratio of water equivalent of snow over ice, $\beta$ is a constant accumulation coefficient, and $Ws$ is the water equivalent of snow over ice in glacier cover areas (in mm). Equation (9) is the mass balance of snow over ice ($M_g$, in mm). Ice melt is calculated by the degree-day method using different degree-day factors ($DDF_g$, in mm °C$^{-1}$ day$^{-1}$) from snow, and the melting process occurs only when there is no snow over ice. $H_g$ is the thickness of a glacier (in mm), and is updated by the balance Equation (11). The area of glacier ($A_g$, in km$^2$) is updated by the volume-area scaling relation using the two parameters $m_g$ and $n_g$ in Equation (12). The glacier volume ($V_g$, in km$^3$) is calculated using the initial glacier area ($A_{g0}$) for each simulation time step.

There are 19 parameters in THREW, as listed in Supplementary Table 7. In this study, the parameters related to snow and glacier are separately calibrated against observational snow and glacier datasets. In the study, we just calibrate the parameters related to the melting rate ($DDF_g$and $DDF_s$) and volume-area scale (i.e., $A$, $WMAX$, $LL$, $n_g$, $m_g$). Other parameters related to snow and glacier use the suggested values in the literature. All the temperature thresholds are assumed as 0 °C, and the ratio of snow transferring to ice is assumed 0.5. Due to the important role of the melt water for the Indus, thresholds related to temperature are automatically calibrated based on PySOT. Calibrated values of temperature thresholds are 4.906 °C, -2.748 °C, and 4.164 °C for $T_{s0}$, $T_{sg}$ and $T_s$ respectively.

## Sensitivity analyses of the glacier module parameters

Glaciers play an important role in hydrological processes over the Tibetan Plateau. To assess the influence of the glacier on the resulting runoff change, we performed a series of sensitivity experiments for the Indus. This is because the Indus has the largest contribution of glacier runoff to total runoff among all seven river basins. Given that the volume-area scaling technique heavily depends on the area of glaciers, a straightforward method, also used by Frey et al. (2014)[14], is adopted to assess the sensitivity of hydrological response to glacier changes. The initial glacier extent was set based on the RGI6.0 (i.e. 19058 $km^2$ glacier area in the year 2012) and a calibrated parameter, the annual glacier changes rate (δ). The range (-0.04 ~ -1.57%/yr) for δ is determined by referring to previous studies[10, 11, 12]. The calibrated value of δ is -1.30%/yr for the Indus. This means that the initial glacier area within the Indus is 30559 $km^2$ at the start of the historical simulation. Considering the glacier evolution, δ of -1.57%/yr and of -0.04%/yr is assumed as the upper and lower bound for uncertainty in the input glacier area, respectively. Besides, the calibrated δ (-1.3%/yr) is changed by ±5%. Another important parameter influencing the results of ice-melt amount is degree-day factors (Equation 10). Similar to the parameter δ, a set of modified degree-day factors (with the calibrated value modified by ±10% and ±5%, respectively) are used. The influence of the δ and degree-day factor on changes in river flows under different warming scenarios are shown in Supplementary Table 11. The non-monotonic changes in river flows are still maintained with varying parameters of the glacier module. We expect our conclusions would also hold with varying parameters of the glacier module for other basins as well, since the contributions of glacier runoff to total runoff are much smaller over other basins than the Indus.

## Supplementary Figures

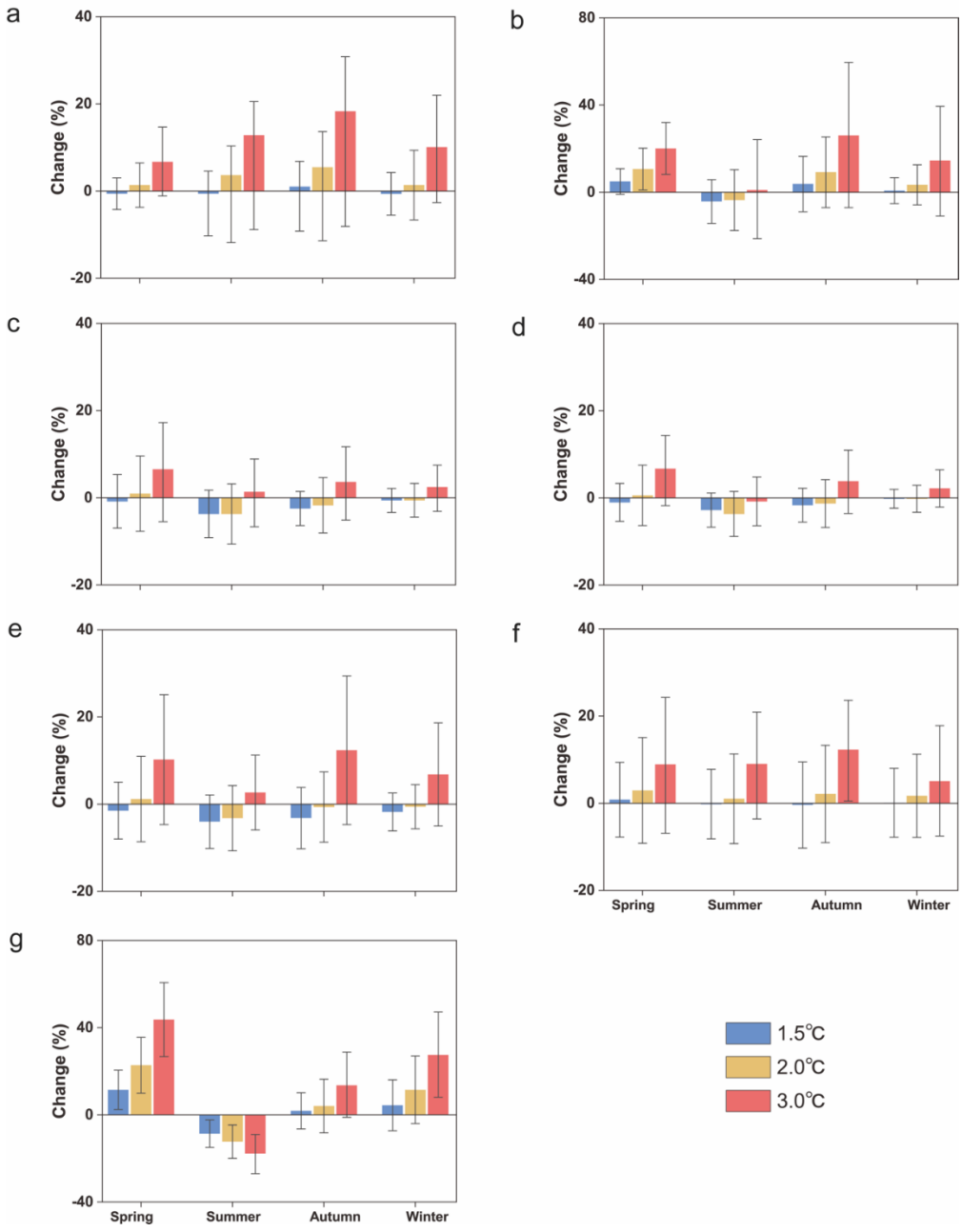


**Supplementary Fig. 1 Relative changes of seasonal river flow at the warming levels of 1.5 °C, 2.0 °C and 3.0 °C for the seven river basins. a** Yellow; **b** Yangtze; **c** Mekong; **d** Salween; **e** Brahmaputra; **f** Ganges; **g** Indus. Color bars represent the ensemble mean from the hydrological simulations driven by the 22 CMIP6 models, while error bars represent one standard deviation. The four seasons are defined as spring (March-May), summer (June-August), autumn (September-October), and winter (November to February of the following year).

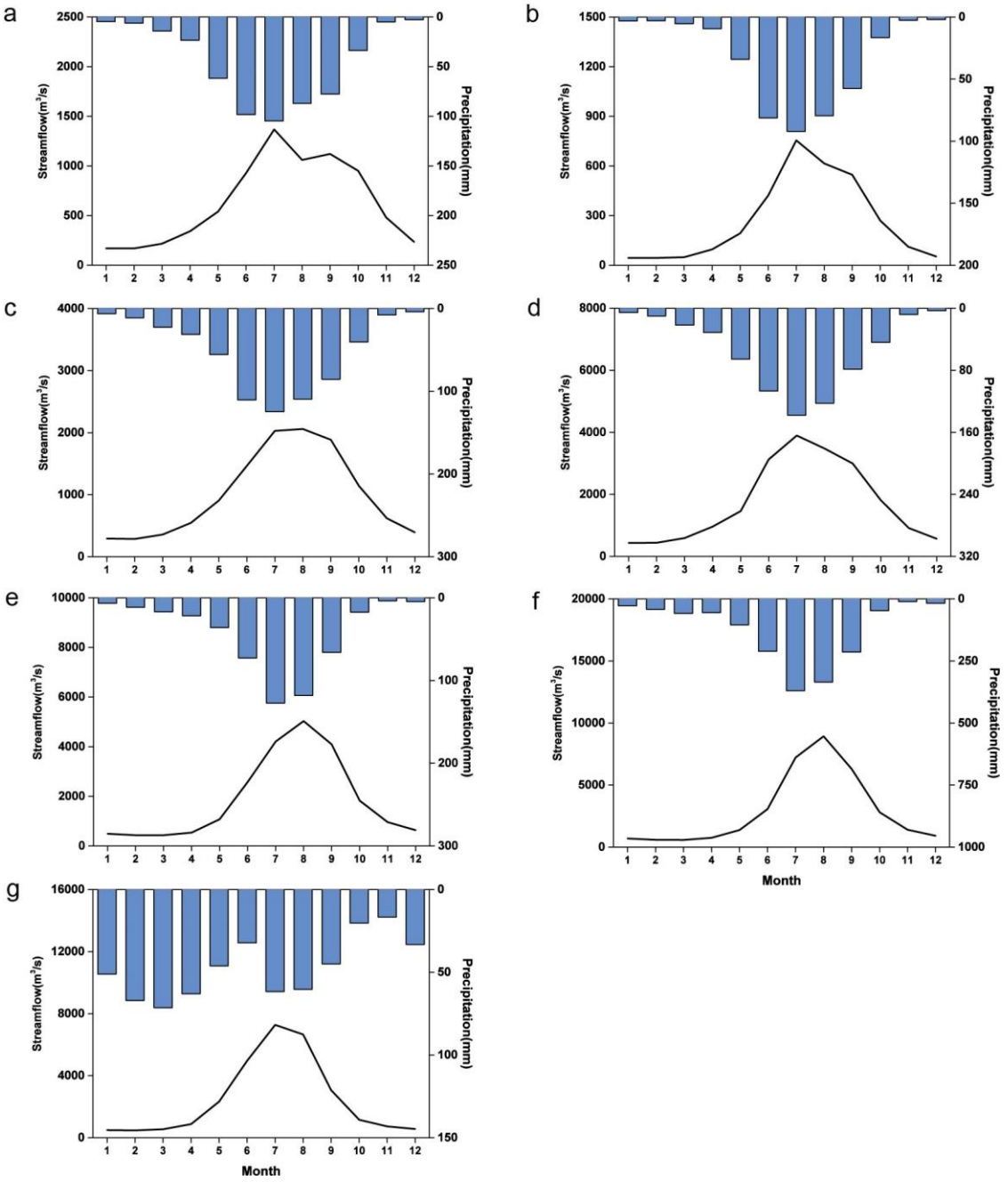


**Supplementary Fig. 2 Monthly streamflow and precipitation of the seven river basins during the historical period.** **a** Yellow; **b** Yangtze; **c** Mekong; **d** Salween; **e** Brahmaputra; **f** Ganges; **g** Indus. Streamflow and precipitation (from the WATCH Forcing Dataset) are calculated within the observed period of streamflow for each river basin (see Supplementary Table 1 for details).

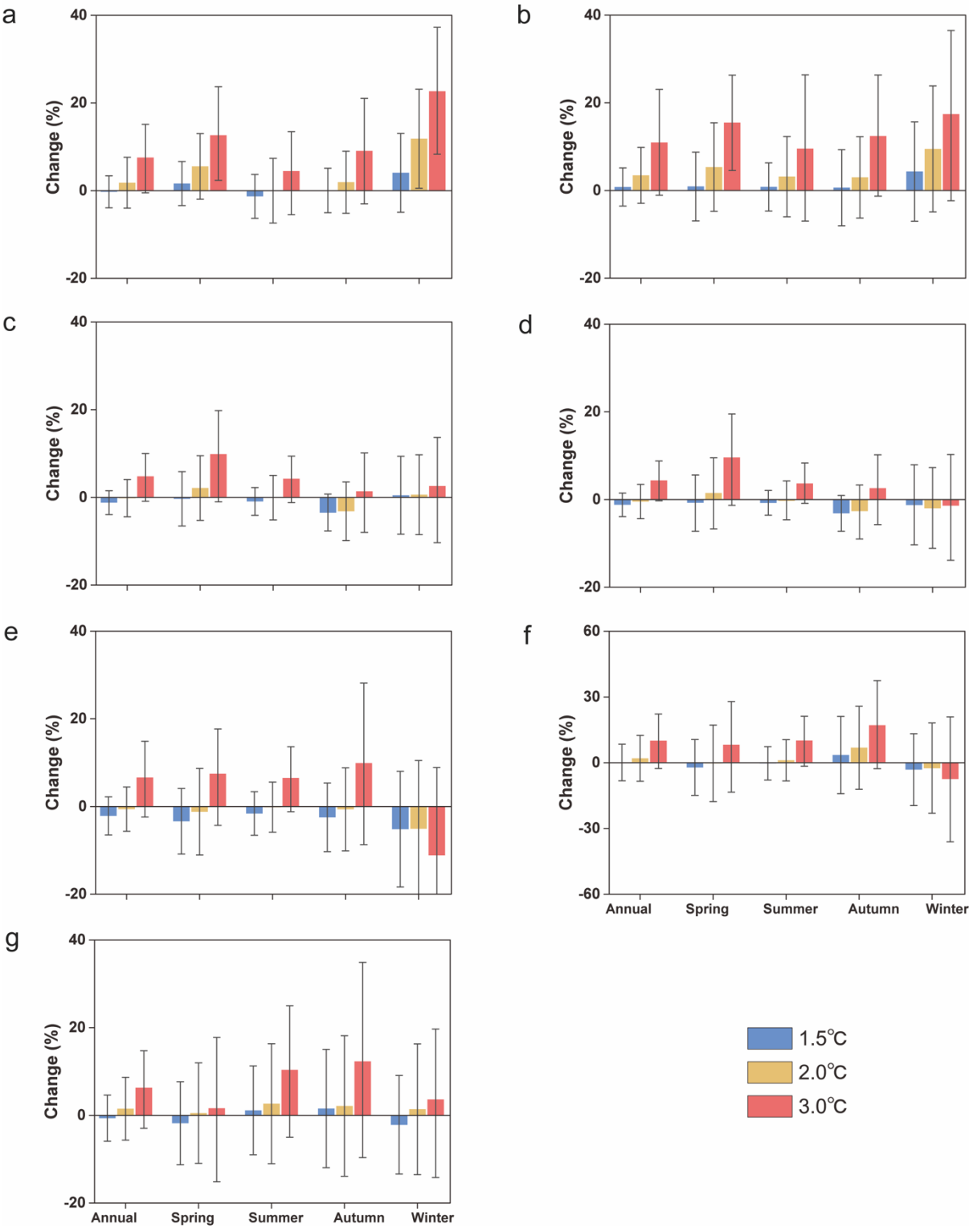


**Supplementary Fig. 3 Relative changes of precipitation at the warming levels of 1.5 °C, 2.0 °C and 3.0 °C for the seven river basins. a** Yellow; **b** Yangtze; **c** Mekong; **d** Salween; **e** Brahmaputra; **f** Ganges; **g** Indus. Color bars represent the ensemble mean from 22 CMIP6 models, while error bars represent one standard deviation

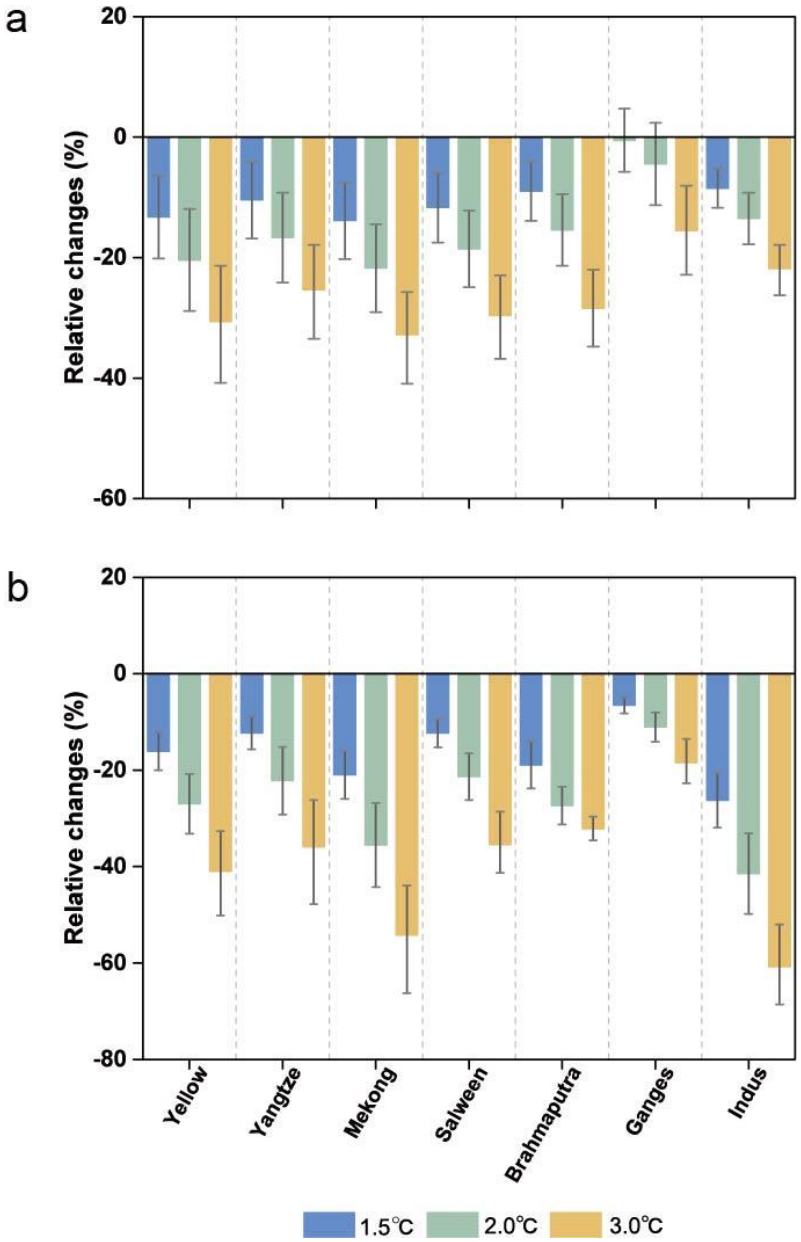


**Supplementary Fig. 4 Relative changes of snow cover and glacier area at the warming levels of 1.5 °C, 2.0 °C and 3.0 °C for the seven river basins. a** percentage of snow cover (PSC); **b** glacier area. Color bars represent the ensemble mean from the hydrological simulations driven by the 22 CMIP6 models, while error bars represent one standard deviation.

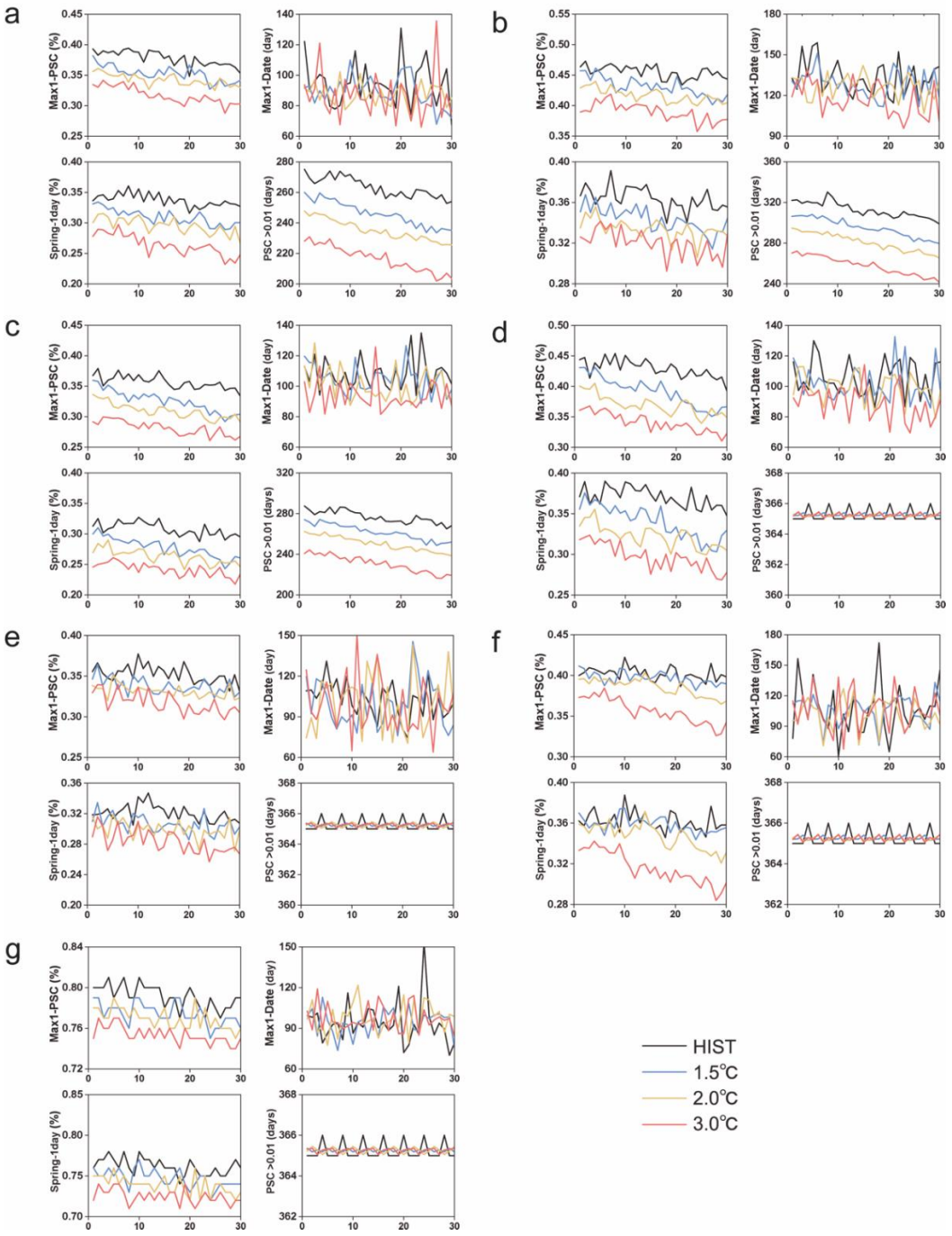


**Supplementary Fig. 5. Variation of the percentage of snow cover (PSC) during the historical period (HIST, 1985-2014) and at the global warming levels of 1.5 °C, 2.0 °C and 3.0 °C for the seven river basins. a** Yellow; **b** Yangtze; **c** Mekong; **d** Salween; **e** Brahmaputra; **f** Ganges; **g** Indus. Max1-PSC: annual 1-day maximum PSC; Max1-Date: Julian date of the annual 1-day maximum PSC; Spring-1day: 1-day maximum PSC in spring. Note that each solid line shows the ensemble mean during a 30-year running period. The grids with PSC exceeding 0.01 are considered.

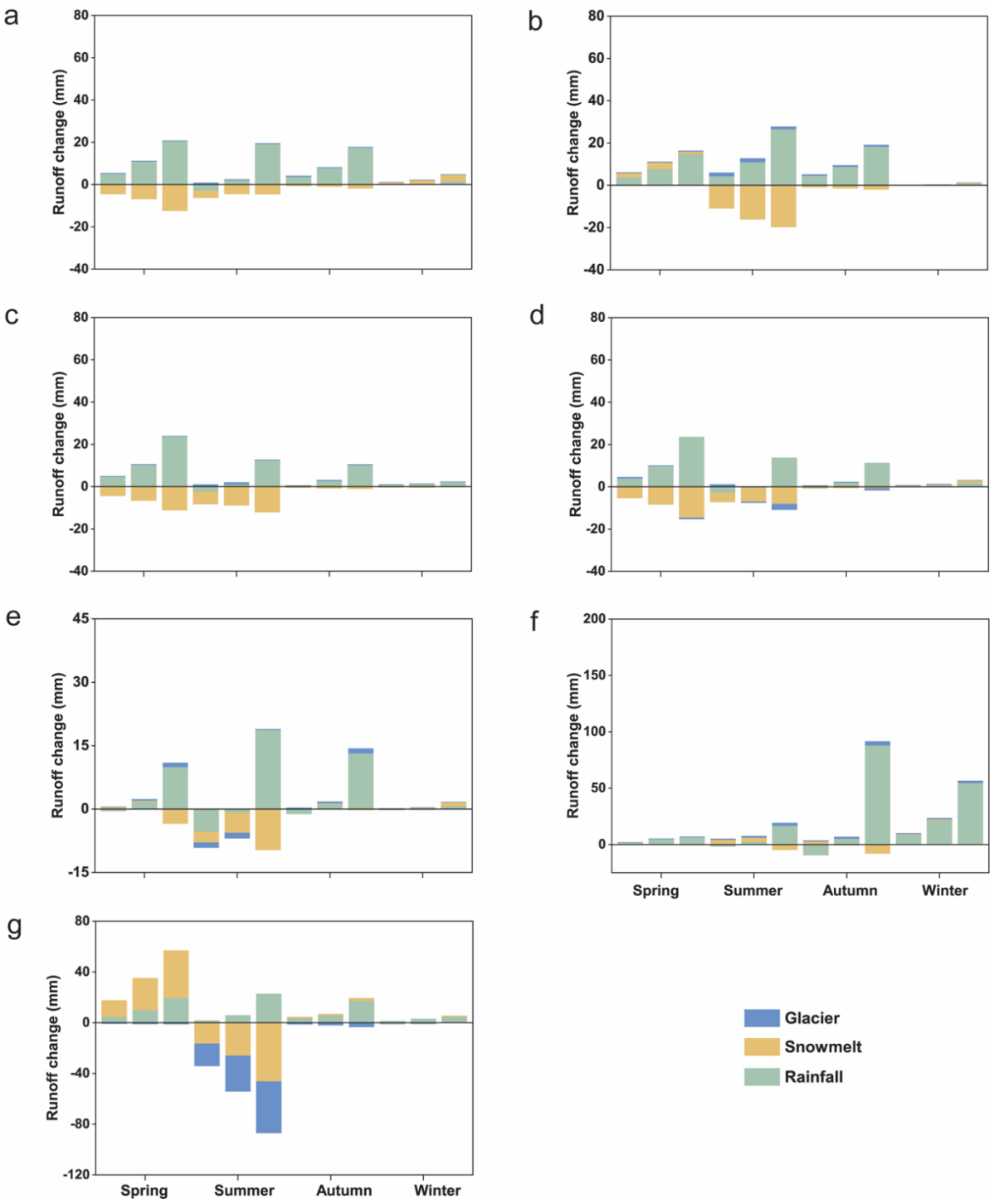


**Supplementary Fig. 6 Relative changes in mean seasonal rainfall runoff, snowmelt runoff, and glacier runoff at the warming levels of 1.5 °C, 2.0 °C and 3.0 °C for the seven river basins**. **a** Yellow; **b** Yangtze; **c** Mekong; **d** Salween; **e** Brahmaputra; **f** Ganges; **g** Indus. Three columns from left to right in each season represent the global warming levels of 1.5 °C, 2.0 °C and 3.0 °C, respectively.

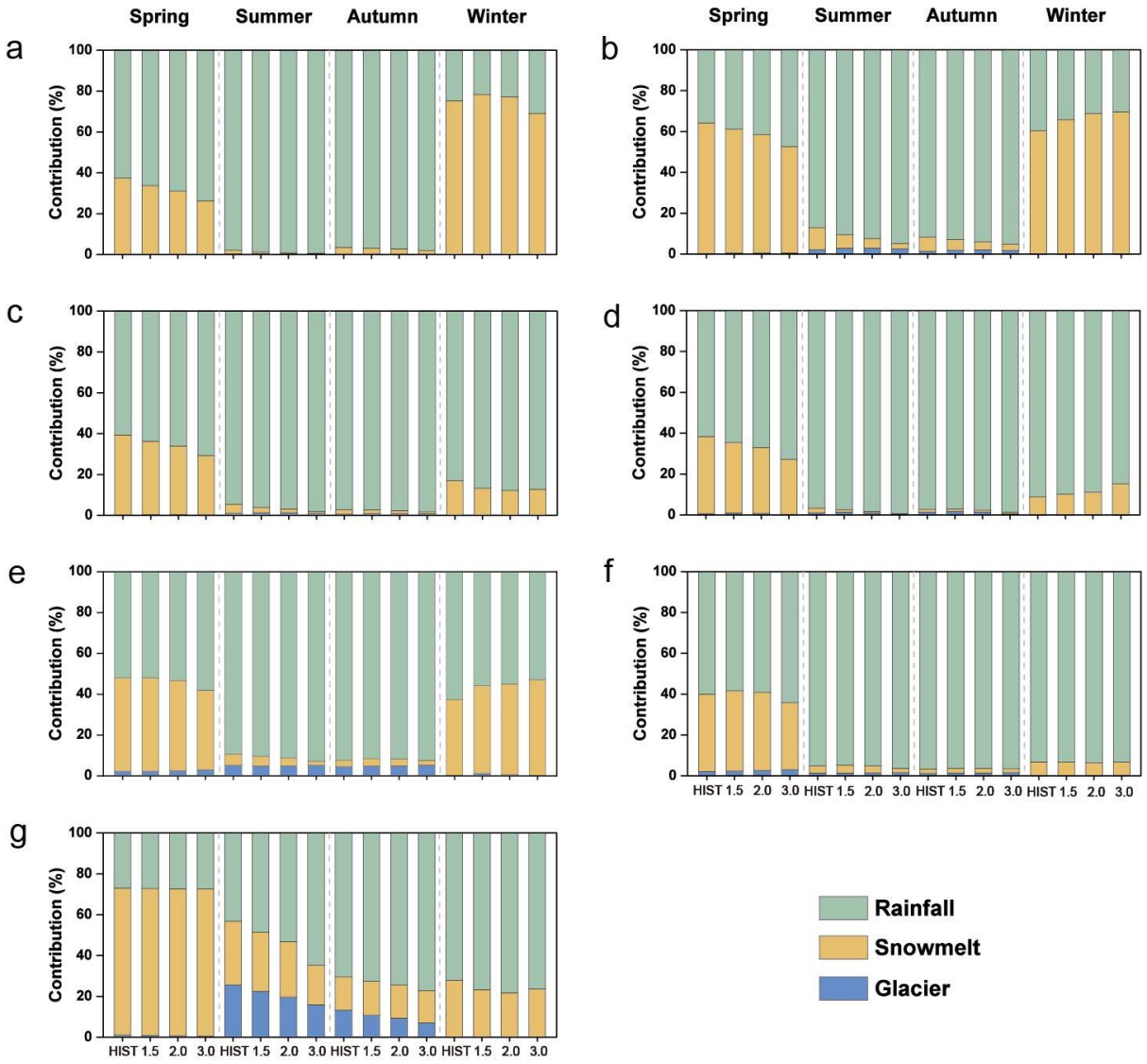


**Supplementary Fig. 7 Relative contribution of different runoff components to seasonal runoff at the warming levels of 1.5 °C, 2.0 °C and 3.0 °C for the seven river basins**. **a** Yellow; **b** Yangtze; **c** Mekong; **d** Salween; **e** Brahmaputra; **f** Ganges; **g** Indus. The first column shows the contribution during the historical period (HIST), while the second to the fourth columns show the contribution at the global warming levels of 1.5 °C, 2.0 °C and 3.0 °C, respectively.

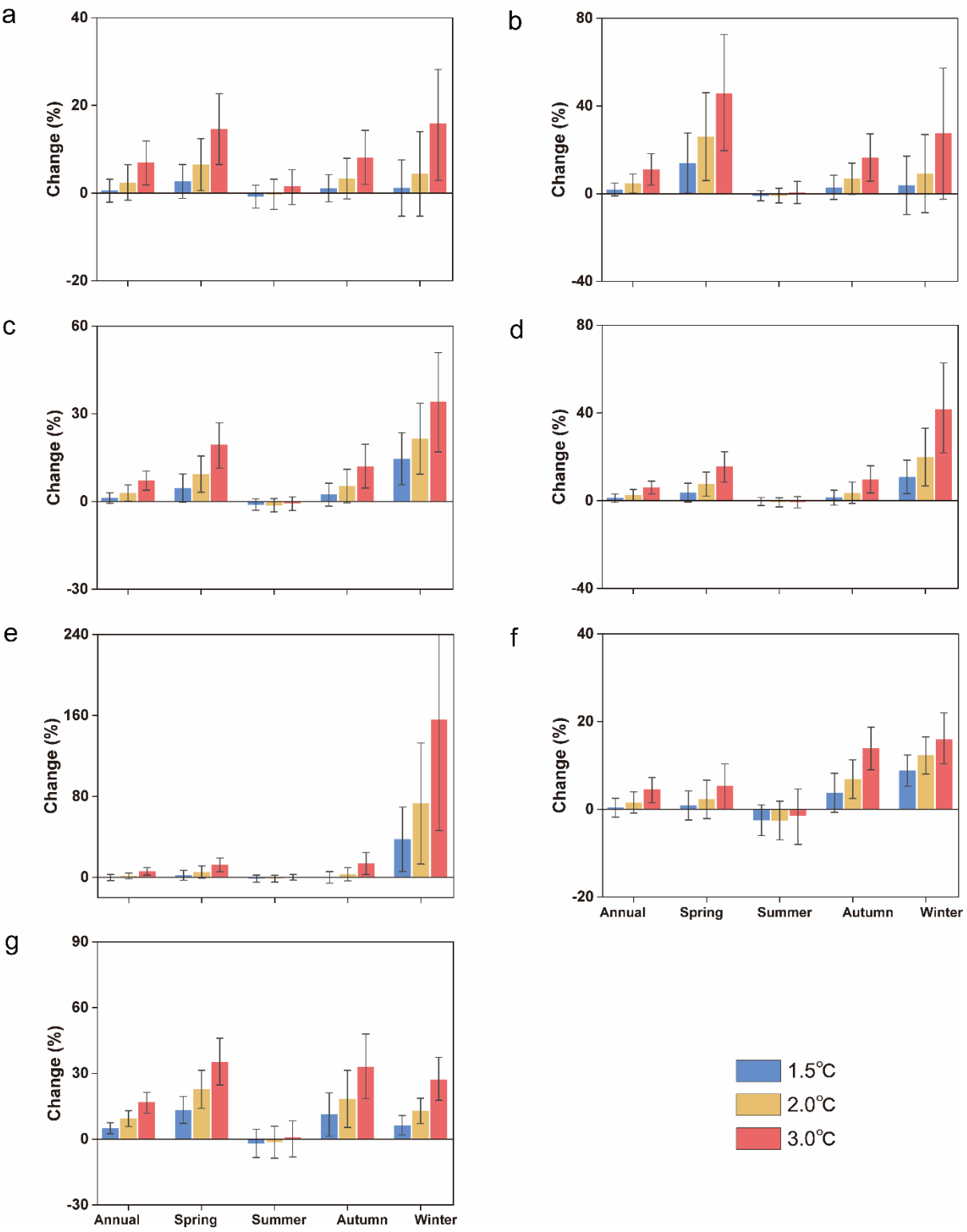


**Supplementary Fig. 8 Relative changes of evapotranspiration at the warming levels of 1.5 °C, 2.0 °C and 3.0 °C for the seven river basins. a** Yellow; **b** Yangtze; **c** Mekong; **d** Salween; **e** Brahmaputra; **f** Ganges; **g** Indus. Color bars represent the ensemble mean from the hydrological simulations driven by the 22 CMIP6 models, while error bars represent one standard deviation.

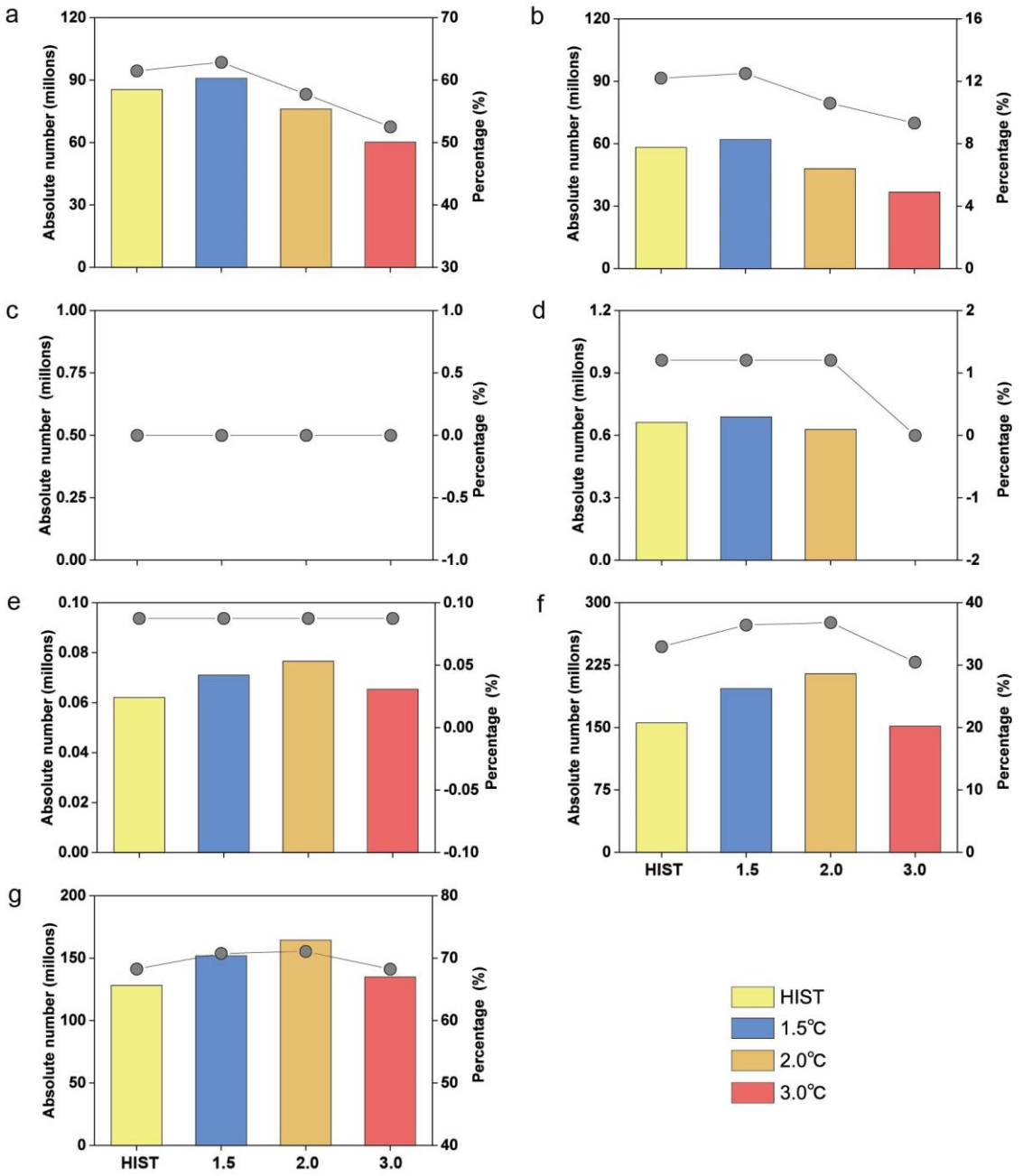


**Supplementary Fig. 9 The absolute number and percentage of people under water scarcity at the global warming levels of 1.5 °C, 2.0 °C and 3.0 °C and during the historical period (HIST) for the seven river basins. a** Yellow; **b** Yangtze; **c** Mekong; **d** Salween; **e** Brahmaputra; **f** Ganges; **g** Indus. Water scarcity conditions are assessed based on the water scarcity index. The grey points are the percentage of the population under water scarcity for the whole basin at different global warming levels. Note that the population under water scarcity for the Mekong (c) is zero.

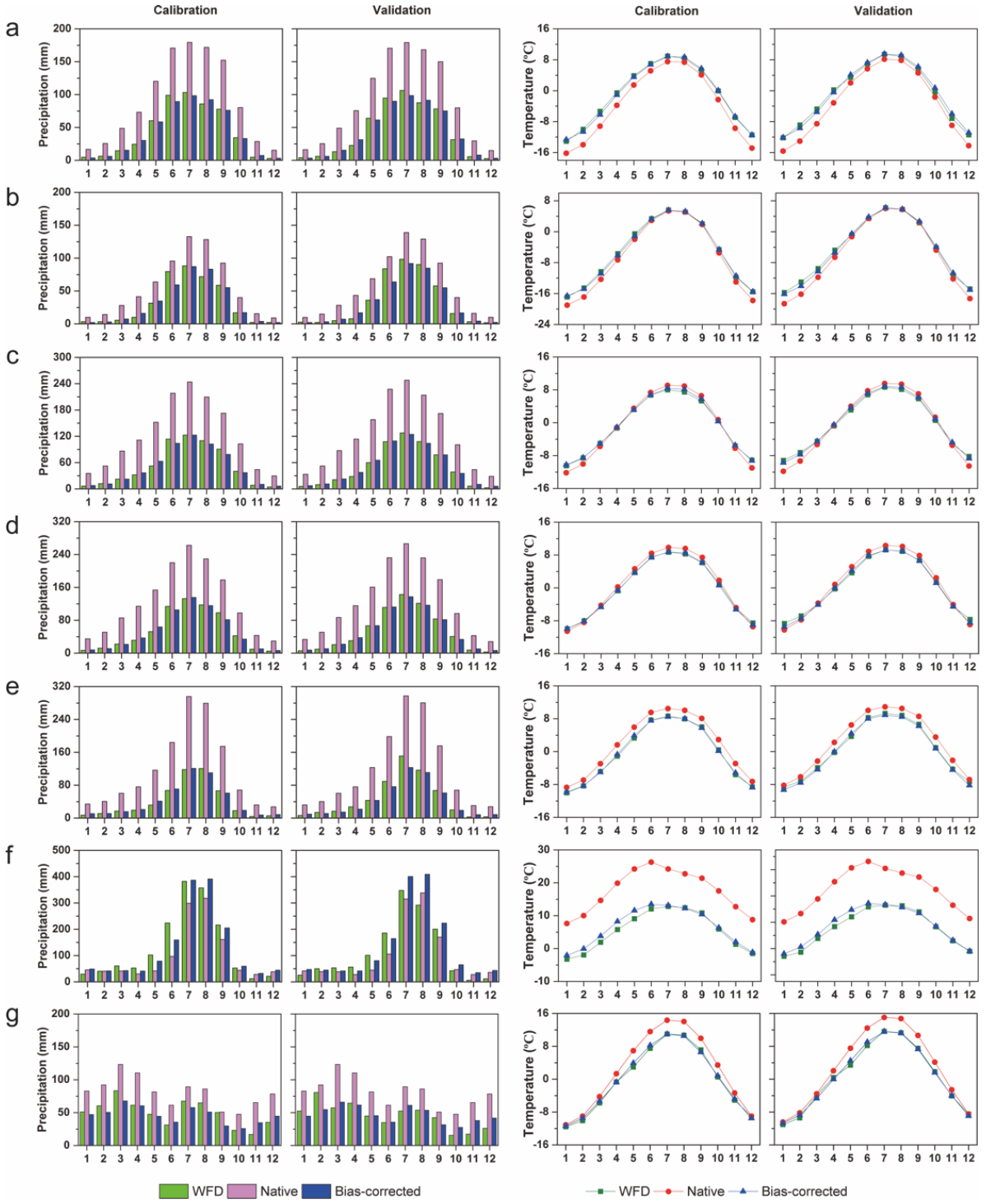


**Supplementary Fig. 10 Seasonal cycles of precipitation and temperature calculated from the WATCH Forcing Dataset (WFD), the ensemble mean of 22 native and bias-corrected CMIP6 model output for the calibration (1980-2000) and validation (2001-2014) period.** **a** Yellow; **b** Yangtze; **c** Mekong; **d** Salween; **e** Brahmaputra; **f** Ganges; **g** Indus. The left two columns represent precipitation, while the right two are temperature.

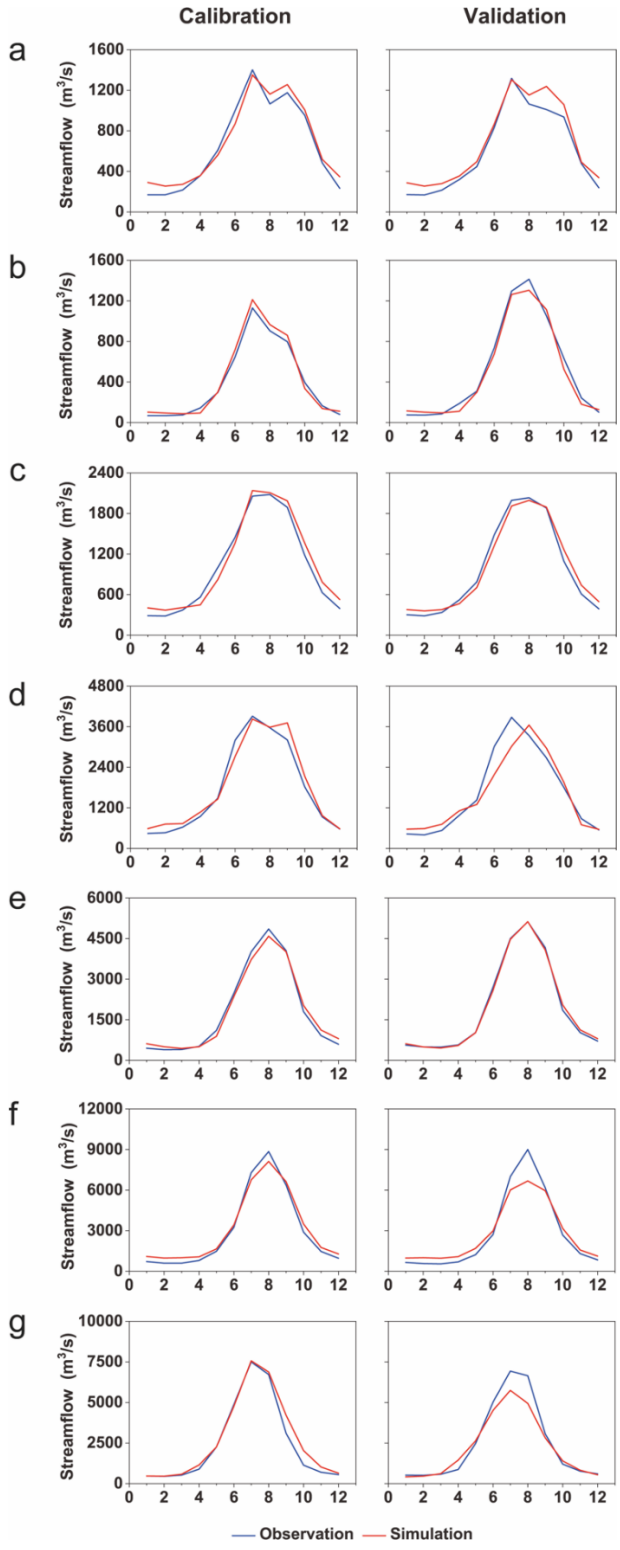


**Supplementary Fig. 11 Comparisons of simulated (in red) and observed (in blue) monthly streamflow for the seven river basins. a** Yellow; **b** Yangtze; **c** Mekong; **d** Salween; **e** Brahmaputra; **f** Ganges; **g** Indus. The left panels show simulated streamflow during the calibration period, while the right panels show results during the validation period.

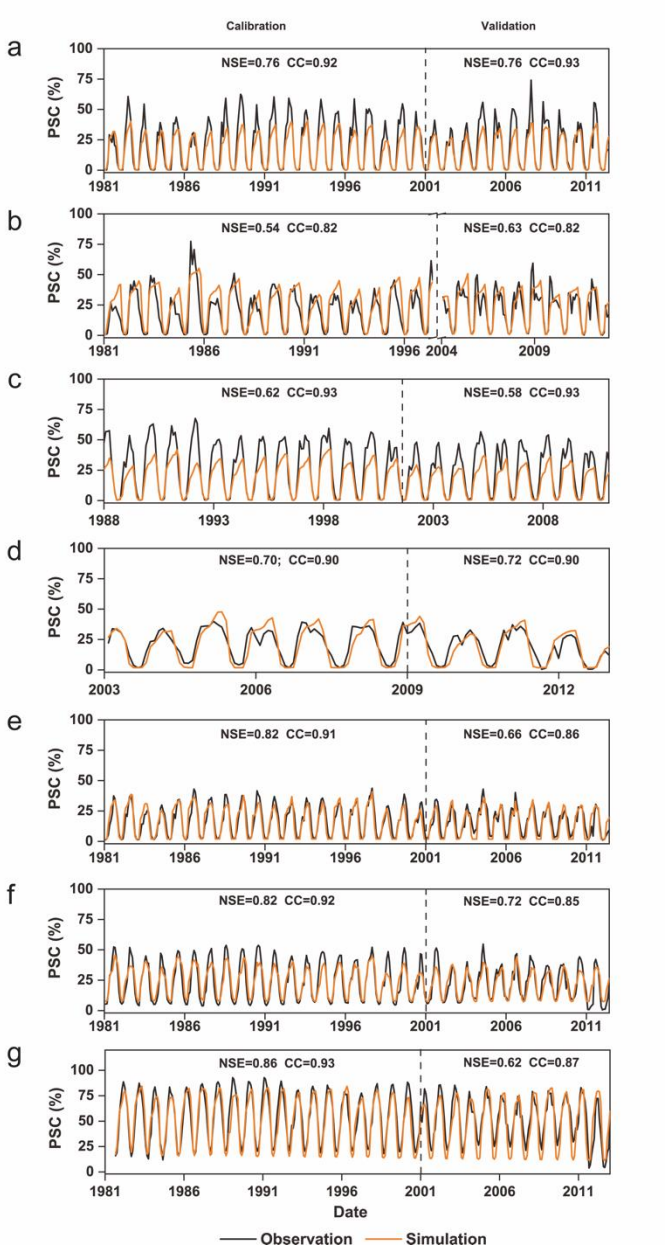


**Supplementary Fig. 12 The observed (black line) and simulated (orange line) monthly percentage of snow cover (PSC) for the seven river basins. a** Yellow; **b** Yangtze; **c** Mekong; **d** Salween; **e** Brahmaputra; **f** Ganges; **g** Indus. The observed snow coverage is provided by the long-term TP daily 5-km cloud-free snow cover extent dataset[15]. The Nash Sutcliffe efficiency coefficient (NSE) and correlation coefficients (CC) values are also shown in the figure.

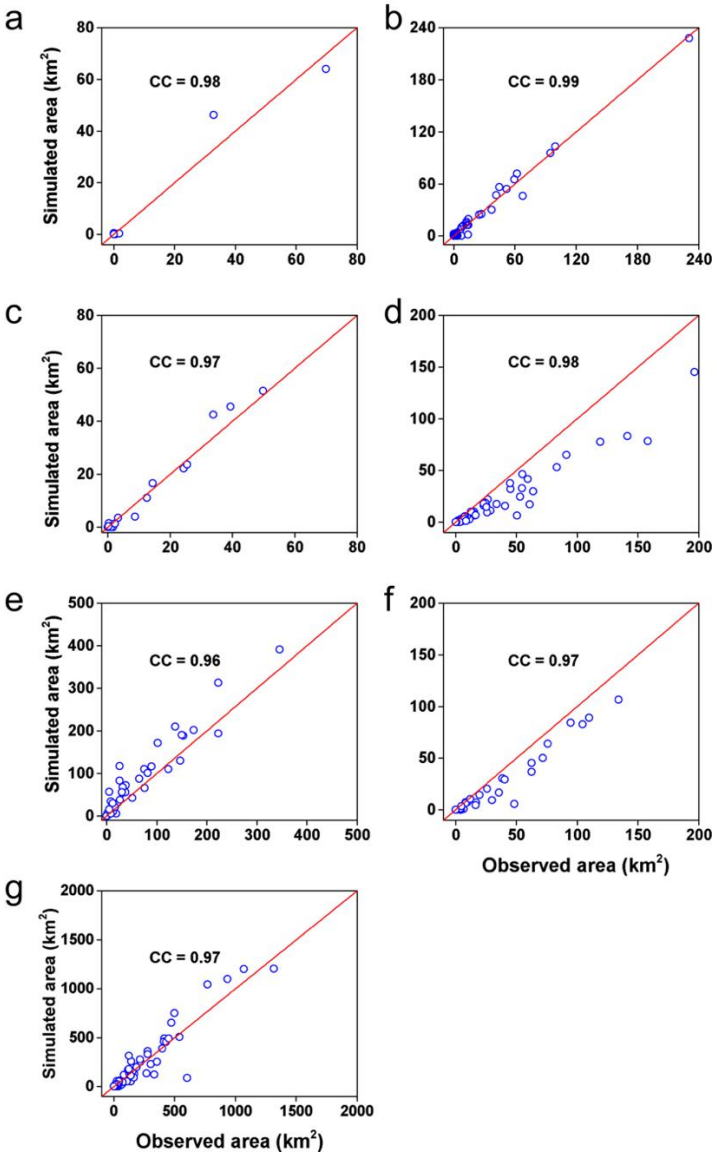


**Supplementary Fig. 13 The correlation coefficients (CC) of the observed and simulated glacier coverage for the REW over the seven river basins. a** Yellow; **b** Yangtze; **c** Mekong; **d** Salween; **e** Brahmaputra; **f** Ganges; **g** Indus. The observed glacier coverage is obtained from the SCGI and RGI6.0.

## Supplementary Tables

**Supplementary Table 1. The main characteristics of the seven river basins over Tibetan Plateau .**

| Basin | Yellow | Yangtze | Mekong | Salween | Brahmaputra | Ganges | Indus |
|---|---|---|---|---|---|---|---|
| Station | Tangnaihai | Zhimenda | Jiuzhou | Daojieba | Nuxia | Devghat/Chisapani | Besham |
| Drainage area ($km^2$) | 121,000 | 137,700 | 88,051 | 110,224 | 205,072 | 80,541 | 164,867 |
| Altitude range (minimum/mean/maximum) (m) | 2656 /4124 /6253 | 3516 /4759 /6575 | 1243 /4323 /6385 | 647 /4486 /6891 | 2914 /4875 /7296 | 129 /3180 /8143 | 361 /4453 /8483 |
| Dominant land covers (%) | Forest 4.5<br>Grassland 93.5<br>Bare 1.1 | Grassland 92.6<br>Bare 5.8<br>Snow and ice 1.3 | Grassland 78.4<br>Forest 17.8<br>Bare area 2.9 | Forest 14.8<br>Grassland 76.3<br>Snow and Ice 4.0 | Grassland 81.4<br>Forest 7.8<br>Snow and Ice 5.0 | Forest 38.6<br>Grassland 27.7<br>Cropland 33.2 | Forest 5.2<br>Grassland 42.8<br>Snow and Ice 46.5 |
| Glacier area ($km^2$) | 106 | 989 | 221 | 1793 | 2632 | 2854 | 19058 |
| Observational period of daily streamflow | 1980-2012 | 1980-1997, 2004-2012 | 1988-2010 | 2003-2012 | 1980-2012 | 1980-2012 | 1980-2012 |
| Streamflow ($m^3/s$) | 631 | 441 | 998 | 1729 | 1858 | 2902 | 2440 |
| Annual Mean temperature (°C) | -1.1 | -5.1 | -0.5 | 0.46 | -0.1 | 4.9 | 0.18 |
| Annual Mean precipitation (mm) | 518 | 386 | 609 | 627 | 503 | 1493 | 575 |
| Runoff ratio | 0.32 | 0.26 | 0.59 | 0.79 | 0.62 | 0.76 | 0.82 |

Note: Streamflow is calculated for the period of streamflow observations; Annual temperature and precipitation are based on the WATCH Forcing Data (WFD); Note that the precipitation in Indus is adjusted by multiplying the WFD by 1.61. Land covers are obtained from Global Land Cover 2000 map by the EC Joint Research Centre (http://bioval.jrc.ec.europa.eu/products/glc2000/glc2000.php).

**Supplementary Table 2. Data from global and regional datasets used for hydrological models in this study.**

| Dataset | Source/Name | Description | Reference and/or Website for download |
|---|---|---|---|
| Climate | WATCH Forcing Data (WFD) | Daily meteorological forcing data at 0.5 arc degree grid global dataset | https://rda.ucar.edu/datasets/[16] |
| Topography | MERIT DEM | Developed by removing multiple error components from the SRTM3[17] and AW3D-30m DEMs[18] | Yamazaki et al. (2014)[19] http://hydro.iis.u-tokyo.ac.jp/~yamadai/MERIT_DEM/ |
| Land use / cover | Daily normalized difference vegetation index (NDVI) | Daily NDVI values at 0.5 arc degree grid derived from Advanced Very High Resolution Radiometer (AVHRR) sensors | Vermote et al. (2019a)[20] https://www.ncei.noaa.gov/products/climate-data-records/normalized-difference-vegetation-index |
| Land use / cover | Leaf Area Index (LAI) | Daily product on a 0.05° by 0.05° grid from 1981 to present derived from Advanced Very High Resolution Radiometer (AVHRR) sensors | Vermote et al. (2019b)[21] https://www.ncei.noaa.gov/products/climate-data-records/leaf-area-index-and-fapar |
| Snow | Long-term TP daily 5-km cloud-free snow cover extent record (TPSCE) | Daily 5-km cloud-free snow cover extent record derived from AVHRR surface reflectance CDR[22] | Chen et al. (2018)[15] |
| Glacier distribution | The First Chinese Glacier Inventory (CGI-1) | Clear and concise overview and scientific assessment of the glaciers in China | Shi et al. (2009)[8] |
| Glacier distribution | The Second Chinese Glacier Inventory (SCGI) | Clear and concise overview and scientific assessment of the glaciers in China | Guo et al. (2015)[23] |
| Glacier distribution | The Randolph Glacier Inventory 6.0 (RGI6.0) | The Randolph Glacier Inventory is a global inventory of glacier outlines. It is supplemental to the Global Land Ice Measurements from Space initiative (GLIMS) | RGI Consortium (2017)[9] |
| Ice Thickness | Ice velocity and thickness of the world's glaciers | The datasets present a comprehensive high-resolution mapping of ice velocity and thickness of more than 98% of the world's glacier | Millan et al. (2022)[13] |

| Dataset | Source/Name | Description | Reference and/or Website for download |
|---|---|---|---|
| Glacier mass balance | Glacier mass balance data | The datasets provided standardized observations on changes in mass, volume, area and length of glaciers over time | World Glacier Monitoring Service (WGMS, 2021)[24] and Hugonnet et al. (2021)[25] |
| Soil | Global high-resolution data set of soil hydraulic and thermal parameters | Optimal soil water retention parameters obtained from ensemble pedotransfer functions | http://globalchange.bnu.edu.cn/research, Dai et al. (2019)[26] |

**Supplementary Table 3. Calibrated and validated results of the THREW model.**

| | | Yellow | Yangtze | Mekong | Salween | Brahmaputra | Ganges | Indus |
|---|---|---|---|---|---|---|---|---|
| Number of REWs | | 215 | 178 | 54 | 355 | 63 | 147 | 74 |
| Average area of REW ($km^2$) | | 657 | 792 | 1677 | 310 | 2971 | 547 | 2227 |
| Calibration period | | 1981-2000 | 1981-1997 | 1988-2000 | 2003-2008 | 1981-2000 | 1981-2000 | 1981-2000 |
| Streamflow (daily/monthly) | NSE | 0.80/0.86 | 0.79/0.86 | 0.86/0.93 | 0.76/0.92 | 0.83/0.88 | 0.87/0.95 | 0.79/0.83 |
| | PBIAS (%) | 5.2/5.2 | 5.3/5.3 | 4.4/4.4 | 4.3/4.4 | -0.1/-0.1 | 5.4/5.5 | 9.7/9.8 |
| | CC | 0.90/0.93 | 0.90/0.93 | 0.93/0.97 | 0.88/0.96 | 0.91/0.94 | 0.93/0.98 | 0.90/0.92 |
| Snow cover (monthly) | NSE | 0.76 | 0.54 | 0.62 | 0.70 | 0.82 | 0.82 | 0.86 |
| | CC | 0.92 | 0.82 | 0.93 | 0.90 | 0.91 | 0.92 | 0.93 |
| Validation period | | 2001-2012 | 2001-2012 | 2001-2010 | 2009-2012 | 2001-2012 | 2001-2012 | 2001-2012 |
| Streamflow (daily/monthly) | NSE | 0.66/0.70 | 0.71/0.75 | 0.89/0.94 | 0.68/0.83 | 0.57/0.59 | 0.81/0.89 | 0.86/0.89 |
| | PBIAS (%) | 12.8/12.8 | -4.7/-4.7 | 1.6/1.6 | -3.0/-3.0 | 0.6/0.6 | -0.8/-0.6 | -9.8/-9.7 |
| | CC | 0.83/0.86 | 0.86/0.88 | 0.94/0.97 | 0.83/0.91 | 0.81/0.82 | 0.92/0.97 | 0.95/0.97 |
| Snow cover (monthly) | NSE | 0.76 | 0.63 | 0.58 | 0.72 | 0.66 | 0.72 | 0.62 |
| | CC | 0.93 | 0.82 | 0.93 | 0.90 | 0.86 | 0.85 | 0.87 |
| Glacier area | PBIAS (%) | 5.39 | -1.89 | 2.05 | -42.20 | 31.6 | -30.4 | -1.82 |
| | CC | 0.98 | 0.99 | 0.97 | 0.98 | 0.96 | 0.97 | 0.97 |

Here the Nash Sutcliffe efficiency coefficient (NSE), correlation coefficient (CC) and percent bias (PBIAS) are used to evaluate the model performance.

**Supplementary Table 4. Details of the 22 CMIP6 climate models used in this study.**

| Model Name | Modeling Center | Realization | Resolution (Lon×Lat) |
|---|---|---|---|
| ACCESS-CM2 | Commonwealth Scientific and Industrial Research Organisation, Australia | r1i1p1f1 | 1.875°×1.25° |
| ACCESS-ESM1-5 | Commonwealth Scientific and Industrial Research Organisation, Australia | r1i1p1f1 | 1.875°×1.2143° |
| BCC-CSM2-MR | Beijing Climate Center and China Meteorological Administration, China | r1i1p1f1 | 1.125°×1.125° |
| CanESM5 | Canadian Centre for Climate Modeling and Analysis, Canada | r1i1p1f1 | 2.8125°×2.8125° |
| CNRM-CM6-1 | National Centre for Meteorological Research and European Centre for Research and Advanced Training in Scientific Computation, France | r1i1p1f2 | 1.40625°×1.40625° |
| CNRM-ESM2-1 | National Centre for Meteorological Research and European Centre for Research and Advanced Training in Scientific Computation, France | r1i1p1f2 | 1.40625°×1.40625° |
| EC-Earth3-Veg | EC-Earth consortium, Europe | r1i1p1f1 | 0.703125°×0.703125° |
| FGOALS-g3 | LASG, Institute of Atmospheric Physics, Chinese Academy of Sciences, China | r1i1p1f1 | 2°×2.25° |
| GFDL-ESM4 | National Oceanic and Atmospheric Administration Geophysical Fluid Dynamics Laboratory, United States | r1i1p1f1 | 1.25°×1° |
| HadGEM3-GC31-LL | Met Office Hadley Centre, UK | r1i1p1f3 | 1.875°×1.25° |
| INM-CM4-8 | Institute for Numerical Mathematics, Russia | r1i1p1f1 | 2°×1.5° |
| INM-CM5-0 | Institute for Numerical Mathematics, Russia | r1i1p1f1 | 2°×1.5° |
| IPSL-CM6A-LR | Institute Pierre Simon Laplace, France | r1i1p1f1 | 2.5°×1.25874° |
| MIROC6 | University of Tokyo, National Institute for Environmental Studies and Japan Agency for Marine-Earth Science and Technology, Japan | r1i1p1f1 | 1.40625°×1.40625° |
| MIROC-ES2L | University of Tokyo, National Institute for Environmental Studies and Japan Agency for Marine-Earth Science and Technology, Japan | r1i1p1f2 | 2.8125°×2.8125° |
| MPI-ESM1-2-HR | Max Planck Institute for Meteorology, Germany | r1i1p1f1 | 0.9375°×0.9375° |
| MPI-ESM1-2-LR | Max Planck Institute for Meteorology, Germany | r1i1p1f1 | 1.875°×1.875° |
| MRI-ESM2-0 | Meteorological Research Institute, Japan | r1i1p1f1 | 1.125°×1.125° |
| NESM3 | Nanjing University of Information Science and Technology, China | r1i1p1f1 | 1.875°×1.875° |
| NorESM2-LM | University of Bergen, Norway | r1i1p1f1 | 2.5°×1.875° |
| NorESM2-MM | Norwegian Climate Centre, Norway | r1i1p1f1 | 1.25°×0.9375° |
| UKESM1-0-LL | Met Office Hadley Centre, UK | r1i1p1f2 | 1.875°×1.25° |

**Supplementary Table 5. Annual mean values of WATCH Forcing Data (WFD)-based precipitation and temperature, the ensemble of 22 native and bias-corrected CMIP6 model output for the calibration (1980-2000) and validation (2001-2014) period.** Note that the precipitation in Indus is adjusted by multiplying the WFD by 1.61.

| | | Yellow | Yangtze | Mekong | Salween | Brahmaputra | Ganges | Indus |
|---|---|---|---|---|---|---|---|---|
| Precipitation (mm, Calibration/Validation) | WFD | 518/515 | 373/405 | 615/593 | 643/642 | 486/558 | 1551/1371 | 592/543 |
| | Native | 1082/1083 | 671/693 | 1458/1479 | 1499/1523 | 1390/1410 | 1184/1230 | 969/986 |
| | Bias-corrected | 513/516 | 370/384 | 603/611 | 630/642 | 497/507 | 1531/1597 | 549/562 |
| Temperature (°C, Calibration/Validation) | WFD | -1.2/-0.8 | -5.3/-4.7 | -0.7/-0.2 | -0.1/0.5 | -0.4/0.5 | 5.4/6.2 | -0.2/0.6 |
| | Native | -3.7/-3.0 | -6.5/-5.9 | -0.8/-0.3 | 0.4/0.9 | 1.7/2.3 | 17.5/17.9 | 2.1/2.8 |
| | Bias-corrected | -1.3/-0.6 | -5.4/-4.8 | -0.6/-0.1 | -0.2/0.3 | -0.3/0.2 | 6.5/6.9 | 0.0/0.7 |

**Supplementary Table 6. The end year of each GCM under SSP245 and SSP585 to obtain specific temperature increases.**

| Models | 1.5°C | | 2°C | | 3°C | |
|---|---|---|---|---|---|---|
| | SSP245 | SSP585 | SSP245 | SSP585 | SSP245 | SSP585 |
| ACCESS-CM2 | 2031 | 2029 | 2041 | 2040 | 2062 | 2058 |
| ACCESS-ESM1-5 | 2031 | 2031 | 2046 | 2044 | 2074 | 2062 |
| BCC-CSM2-MR | 2035 | 2032 | 2049 | 2043 | 2094 | 2064 |
| CanESM5 | 2027 | 2027 | 2036 | 2035 | 2056 | 2050 |
| CNRM-CM6-1 | 2039 | 2037 | 2054 | 2048 | 2084 | 2066 |
| CNRM-ESM2-1 | 2035 | 2034 | 2055 | 2048 | 2084 | 2069 |
| EC-Earth3-Veg | 2035 | 2032 | 2052 | 2044 | 2080 | 2064 |
| FGOALS-g3 | 2039 | 2037 | 2061 | 2055 | - | 2078 |
| GFDL-ESM4 | 2035 | 2038 | 2057 | 2053 | - | 2075 |
| HadGEM3-GC31-LL | 2025 | 2025 | 2034 | 2033 | 2054 | 2049 |
| INM-CM4-8 | 2042 | 2038 | 2060 | 2051 | - | 2073 |
| INM-CM5-0 | 2038 | 2035 | 2062 | 2048 | - | 2072 |
| IPSL-CM6A-LR | 2032 | 2032 | 2044 | 2044 | 2068 | 2061 |
| MIROC6 | 2040 | 2038 | 2056 | 2052 | - | 2073 |
| MIROC-ES2L | 2036 | 2036 | 2053 | 2047 | 2093 | 2068 |
| MPI-ESM1-2-HR | 2036 | 2037 | 2058 | 2053 | - | 2076 |
| MPI-ESM1-2-LR | 2043 | 2041 | 2060 | 2056 | - | 2077 |
| MRI-ESM2-0 | 2032 | 2029 | 2046 | 2040 | 2076 | 2061 |
| NESM3 | 2028 | 2027 | 2041 | 2037 | 2071 | 2056 |
| NorESM2-LM | 2043 | 2041 | 2068 | 2058 | - | 2080 |
| NorESM2-MM | 2042 | 2039 | 2061 | 2053 | - | 2078 |
| UKESM1-0-LL | 2027 | 2027 | 2036 | 2035 | 2052 | 2048 |
| Average | 2035 | 2034 | 2051 | 2046 | 2073 | 2066 |

**Supplementary Table 7. Details of the THREW model parameters.**

| Symbol | Unit | Description | Range |
|---|---|---|---|
| kv | | Fraction of potential transpiration rate over potential evaporation | 0.001~0.8 |
| nt | - | Manning roughness coefficient of hillslope | 0.0001~0.2 |
| GaIFL | - | Spatial heterogeneous coefficient of infiltration capacity | 0.001~0.7 |
| GaEFL | - | Spatial heterogeneous coefficient of exfiltration capacity | 0.0001~0.7 |
| GaETL | - | Spatial heterogeneous coefficient of evapotranspiration capacity | 0.0001~0.7 |
| WM | | Tension water storage capacity | 0.1~10 |
| B | - | Shape coefficient for calculating the saturation excess streamflow area | 0.001~1 |
| Gatr | | Coefficient representing spatial heterogeneity of exchange term between t-zone and r-zone | 0.001~10 |
| KKA | - | Coefficient for calculating subsurface flow in $R_g=KKD\cdot S\cdot K_S^S(\frac{y^S}{Z})^{KKA}$, When $S$ is the topographic slope, $y^S$ is the depth of zone, $Z$ is the total soil depth | 0.01~6 |
| KKD | - | See describe for $KKA$ | 0.0001~0.5 |
| $DDF_S$ | mm °C$^{-1}$ day$^{-1}$ | Degree day factor for snow | 0.001~10 |
| C1 | - | Coefficient for calculating the runoff concentration process using Muskingum method: $O_2=C_1\cdot I_1+C_2\cdot I_2+C_3\cdot O_1+C_4\cdot Q_{lat}O_2=C_1\cdot I_1+C_2\cdot I_2+C_3\cdot O_1+C_4\cdot Q_{lat}$, where $I_1$ and $O_1$ is the inflow and outflow at the prior step, $I_2$ and $O_2$ is the inflow and outflow at current step, $Q_{lat}$ is the lateral flow of the river channel, $C_3=1-C_1-C_2$, $C_4=C_1+C_2$ | 0.0001~1 |
| C2 | - | See description for $C_1$ | 0.0001~1 |
| LL | - | Coefficient used in snow depletion curve for calculating snow cover area in $SCA=A\cdot(\frac{SWE}{WMAX})^{LL}$ | 0.0001~1 |
| WMAX | mm | See description for $LL$ | 0.001~10 |
| A | - | See description for $LL$ | 0.001~10 |
| $m_g$ | - | Parameters in glacier volume-area scaling relation $A_g=(\frac{V_g}{m_g})^{ng}$ | 0.001~10 |
| $n_g$ | - | See description for mg | 0.001~10 |
| $DDF_G$ | mm °C$^{-1}$ day$^{-1}$ | Degree day factor for glacier | 0.001~10 |

**Supplementary Table 8. The criteria used to evaluate the model performance in this study.**

| Name | Formula | Range | Ideal value |
|---|---|---|---|
| Nash Sutcliffe efficiency coefficient (NSE) | $NSE = 1 - \frac{\sum_{t=1}^{n}(Q_{s,t} - Q_{o,t})^2}{\sum_{t=1}^{n}(Q_{o,t} - \overline{Q_o})^2}$ | (-∞,1) | 1 |
| Correlation coefficient (CC) | $CC = \frac{\sum_{t=1}^{n}(Q_{s,t} - \overline{Q_s}) \cdot (Q_{o,t} - \overline{Q_o})}{\sqrt{\sum_{t=1}^{n}(Q_{s,t} - \overline{Q_s})^2 \cdot \sum_{t=1}^{n}(Q_{o,t} - \overline{Q_o})^2}}$ | (-1,1) | 1 |
| Percent bias (PBIAS) | $PBIAS = \frac{\sum_{t=1}^{n}(Q_{s,t} - Q_{o,t})}{\sum_{t=1}^{n} Q_{o,t}} \cdot 100$ | (-∞,+∞) | 0 |

Note that: $Q_{o,t}$ and $Q_{s,t}$ are the sequence of observed and simulated variables, respectively; $\overline{Q_o}$ and $\overline{Q_s}$ are mean values of the observed and simulated variables, respectively; $n$ denotes the total number of days in the calibration period.

**Supplementary Table 9. The optimal value of the THREW model parameters.**

| Parameter | Yellow | Yangtze | Mekong | Salween | Brahmaputra | Ganges | | Indus |
|---|---|---|---|---|---|---|---|---|
| | | | | | | Karnali | Gandaki | |
| kv | 0.492 | 0.702 | 0.56 | 0.771 | 0.780 | 0.101 | 0.655 | 0.611 |
| nt | 0.107 | 0.182 | 0.152 | 0.147 | 0.051 | 0.001 | 0.085 | 0.005 |
| GaIFL | 0.142 | 0.665 | 0.081 | 0.305 | 0.644 | 0.111 | 0.57 | 0.628 |
| GaEFL | 0.341 | 0.537 | 0.508 | 0.214 | 0.550 | 0.447 | 0.623 | 0.483 |
| GaETL | 0.606 | 0.363 | 0.302 | 0.59 | 0.497 | 0.115 | 0.7 | 0.335 |
| WM | 4.203 | 7.38 | 4.034 | 7.445 | 2.492 | 9.638 | 8.7 | 4.707 |
| B | 0.202 | 0.83 | 0.282 | 0.924 | 0.224 | 0.015 | 0.079 | 0.011 |
| Gatr | 0.057 | 0.055 | 1.169 | 1.942 | 7.736 | 7.195 | 8.364 | 8.416 |
| KKA | 4.942 | 5.299 | 3.78 | 1.812 | 5.603 | 5.479 | 5.459 | 1.109 |
| KKD | 0.008 | 0.005 | 0.099 | 0.002 | 0.190 | 0.245 | 0.435 | 0.087 |
| $DDF_S$ | 9.743 | 9.106 | 6.533 | 5.035 | 5.683 | 3.107 | 8.534 | 4.938 |
| C1+C2 | 0.604 | 0.729 | 0.266 | 0.912 | 0.084 | 0.636 | 0.164 | 0.594 |
| C1/(C1+ C2) | 0.308 | 0.623 | 0.812 | 0.439 | 0.064 | 0.488 | 0.047 | 0.426 |
| LL | 0.587 | 0.514 | 0.714 | 0.737 | 0.368 | 0.097 | 0.924 | 0.172 |
| WMAX | 4.06 | 2.69 | 3.995 | 1.798 | 1.468 | 1.457 | 4.803 | 1.317 |
| A | 4.096 | 2.63 | 5.041 | 4.228 | 1.014 | 0.778 | 8.599 | 1.089 |
| $m_g$ | 2.796 | 1.932 | 0.725 | 0.788 | 1.734 | 0.713 | 0.698 | 4.972 |
| $n_g$ | 1.326 | 1.324 | 1.388 | 1.29 | 1.402 | 1.55 | 1.396 | 1.200 |
| $DDF_G$ | 4.540 | 5.100 | 5.298 | 2.454 | 2.768 | 1.658 | 4.619 | 3.729 |

**Supplementary Table 10. Comparison of the glacier mass balance between this study and results extracted from two other different datasets for the Brahmaputra and Indus.**

| No. of REW | Brahmaputra | | | | Indus | | | |
|---|---|---|---|---|---|---|---|---|
| | WGMS (m/yr) | Hugonnet et al. (2021) (m/yr) | Results from this study (m/yr) | Period | WGMS (m/yr) | Hugonnet et al. (2021) (m/yr) | Results from this study (m/yr) | Period |
| 1 | -0.025 | -0.831 | -0.079 | 2000-2010 | 0.098 | 0.116 | -0.128 | 2000-2008 |
| 2 | -0.954 | -0.704 | -0.397 | 2000-2010 | -0.178 | 0.159 | -0.185 | 2000-2008 |
| 3 | | | | | -0.551 | 0.178 | -0.133 | 2000-2008 |
| 4 | | | | | -0.174 | -0.084 | -0.705 | 2000-2008 |
| 5 | | | | | -0.037 | -0.067 | -0.212 | 2000-2010 |
| 6 | | | | | 0.35 | 0.02 | -0.496 | 2000-2010 |
| 7 | | | | | -0.145 | | -0.346 | 1999-2007 |
| 8 | | | | | -0.554 | -0.273 | -1.033 | 2000-2011 |
| 9 | | | | | -0.775 | -0.401 | -0.549 | 2000-2011 |
| Average | -0.489 | -0.767 | -0.238 | | -0.218 | -0.044 | -0.421 | |

**Supplementary Table 11.** Sensitivity assessment of future runoff change to different parameters for Indus river.

| Different scenario | | Future runoff change compared to baseline period | | |
|---|---|---|---|---|
| | | 1.5 °C | 2.0 °C | 3.0°C |
| Baseline | $\delta = 1.60$<br>$DDF_G = 3.729$ | -2.46% | -1.85% | 1.45% |
| Annual glacier change rate ($\delta$) | The upper bound (1.71) | -2.59% | -2.09% | 1.09% |
| | The lower bound (1.01) | -1.83% | -0.62% | 3.28% |
| | +5% (1.68) | -2.55% | -2.03% | 1.19% |
| | -5% (1.52) | -2.37% | -1.68% | 1.71% |
| Degree-day factors ($DDF_G$) | The upper bound (4.102) | -3.03% | -2.69% | 0.24% |
| | The lower bound (3.356) | -1.88% | -0.98% | 2.74% |
| | +5% (3.915) | -2.74% | -2.27% | 0.83% |
| | -5% (3.543) | -2.17% | -1.42% | 2.09% |

## Supplementary References


1. van Pelt SC, Kabat P, ter Maat HW, van den Hurk BJJM, Weerts AH. Discharge simulations performed with a hydrological model using bias corrected regional climate model input. *Hydrol. Earth Syst. Sci* **13**,2387-2397 (2009).

2. Parajka J, Bloschl G. The value of MODIS snow cover data in validating and calibrating conceptual hydrologic models. *J. Hydrol* **358**,240-258 (2008).

3. He ZH, Parajka J, Tian FQ, Bloschl G. Estimating degree-day factors from MODIS for snowmelt runoff modeling. *Hydrol. Earth Syst. Sci* **18**,4773-4789 (2014).

4. Nan Y, Tian LD, He ZH, Tian FQ, Shao LL. The value of water isotope data on improving process understanding in a glacierized catchment on the Tibetan Plateau. *Hydrol. Earth Syst. Sci* **25**,3653-3673 (2021).

5. Luo Y, Arnold J, Liu SY, Wang XY, Chen X. Inclusion of glacier processes for distributed hydrological modeling at basin scale with application to a watershed in Tianshan Mountains, northwest China. *J. Hydrol* **477**,72-85 (2013).

6. Hock R, Jansson P, Braun LN. Modelling the response of mountain glacier discharge to climate warming. In: *Global change and mountain regions: An Overview of Current Knowledge*. (Springer, Dordrecht, 2005).

7. Chen J, Ohmura A. Estimation of Alpine glacier water resources and their change since the 1870s. *IAHS publ* **193**,127-135 (1990).

8. Shi Y, Liu C, Kang E. The glacier inventory of China. *Ann. Glaciol* **50**,1-4 (2009).

9. RGI Consortium. Randolph Glacier inventory–A dataset of Global glacier outlines: Version 6.0: Technical report, Global land ice measurements from space. https://doi.org/10.7265/N5-RGI-60. (2017)

10. Bolch T, *et al*. Status and change of the cryosphere in the extended Hindu Kush Himalaya region. In: *The Hindu Kush Himalaya Assessment*. (Springer International Publishing, Cham, Switzerland, 2019).

11. Huang L, Li Z, Zhou JM, Zhang P. An automatic method for clean glacier and nonseasonal snow area change estimation in High Mountain Asia from 1990 to 2018. *Remote Sens. Environ* **258**,112376 (2021).

12. Ninglian W, Tandong Y, Baiqing X, An'an C, Weicai W. Spatiotemporal pattern, trend, and influence of glacier change in Tibetan Plateau and surroundings under global warming. *Bulletin of Chinese Academy of Sciences (Chinese Version)* **34**,1220-1232 (2019).

13. Millan R, Mouginot J, Rabatel A, Morlighem M. Ice velocity and thickness of the world's glaciers. *Nat. Geosci* **15**,124-129 (2022).

14. Frey H, *et al*. Estimating the volume of glaciers in the Himalayan–Karakoram region using different methods. *The Cryosphere* **8**,2313-2333 (2014).

15. Chen XN, *et al*. Developing a composite daily snow cover extent record over the Tibetan Plateau from 1981 to 2016 using multisource data. *Remote Sens. Environ* **215**,284-299 (2018).

16. Hadley Centre for Climate Prediction and Research. WATer and global CHange (WATCH) Forcing Data (WFD) - 20th Century. https://rda.ucar.edu/datasets/. (2018)

17. Farr TG, *et al*. The shuttle radar topography mission. *Rev. Geophys* **45** (2007).

18. Tadono T, *et al*. Generation of the 30 M-Mesh Global Digital Surface Model by Alos Prism. *Int Arch Photogramm* **41**,157-162 (2016).

19. Yamazaki D, Ikeshima D, Sosa J, Bates PD, Allen GH, Pavelsky TM. MERIT Hydro: A High-Resolution Global Hydrography Map Based on Latest Topography Dataset. *Water Resour. Res* **55**,5053-5073 (2019).

20. Vermote E. NOAA Climate Data Record (CDR) of AVHRR Normalized Difference Vegetation Index (NDVI), Version 5. https://www.ncei.noaa.gov/products/climate-data-records/normalized-difference-vegetation-index (2019).

21. Vermote E. NOAA Climate Data Record (CDR) of AVHRR Leaf Area Index (LAI) and Fraction of Absorbed Photosynthetically Active Radiation (FAPAR), Version 5. https://www.ncei.noaa.gov/products/climate-data-records/leaf-area-index-and-fapar. (2019)

22. Vermote E, *et al*. NOAA Climate Data Record (CDR) of AVHRR Surface Reflectance, Version 5. http://dx.doi.org/10.7289/V5TM782M. (2019)

23. Guo WQ, *et al*. The second Chinese glacier inventory: data, methods and results. *J Glaciol* **61**,357-372 (2015).

24. WGMS. Fluctuations of Glaciers Database. http://dx.doi.org/10.5904/wgms-fog-2021-05 (2021).

25. Hugonnet R, *et al*. Accelerated global glacier mass loss in the early twenty-first century. *Nature* **592**,726-731 (2021).

26. Dai Y, *et al*. A Global High‐Resolution Data Set of Soil Hydraulic and Thermal Properties for Land Surface Modeling. *J. Adv. Model. Earth Syst* **11**,2996-3023 (2019).